PERPENDICULAR SHOCK REFORMATION AND ION ACCELERATION

S. C. CHAPMAN[1,*], R. E. LEE[1] and R. O. DENDY[1,2]
[1] *Space and Astrophysics Group and Centre for Scientific Computing, University of Warwick, Coventry CV4 7AL, U.K.*
[2] *UKAEA Culham Division, Culham Science Centre, Abingdon, Oxon OX14 3DB, U.K.*
*(*Author for correspondence, e-mail: S.C.Chapman@warwick.ac.)*

(Received 27 August 2005; Accepted in final form 27 October 2005)

Abstract. Kinetic simulations of supercritical, quasi-perpendicular shocks yield time-varying solutions that cyclically reform on proton spatio-temporal scales. Whether a shock solution is stationary or reforming depends upon the plasma parameters which, for SNR shocks and the heliospheric termination shock, are ill defined but believed to be within this time-dependent regime. We first review the time-dependent solutions and the acceleration processes of the ions for a proton–electron plasma. We then present recent results for a three-component plasma: background protons, electrons and a second ion population appropriate for SNR (heavy ions) or the termination shock (pickup protons). This ion acceleration generates a suprathermal "injection" population – a seed population for subsequent acceleration at the shock, which may in turn generate ions at cosmic ray energies.

Keywords: collisionless shocks, cosmic rays, supernovae remnants, heliospheric termination shock

1. Introduction

The acceleration of particles to cosmic ray energies is an outstanding problem in space and astrophysical plasmas. One mechanism of interest is diffusive acceleration at Supernova Remnant (SNR) shocks (Bell, 1978). A related question is the generation of anomalous cosmic rays (ACR) at the heliospheric termination shock (Fisk *et al.*, 1974; Pesses *et al.*, 1981; see also Kucharek and Scholer, 1995; Zank *et al.*, 1996; Ellison *et al.*, 1999; Rice *et al.*, 2000; Lever *et al.*, 2001; Zank *et al.*, 2001). Before acceleration to high energies can occur, particles must first be accelerated above the energies of the background plasma so that they may then execute repeated scattering across the shock. This "injection process" requires consideration of plasma phenomena which occur locally to the shock, for which fully self-consistent numerical simulations are possible. Particle in cell (PIC) simulations of quasi-perpendicular shocks (see, e.g., Biskamp and Welter, 1972; Lembège and Dawson, 1987; Lembège and Savoini, 1992; Shimada and Hoshino, 2000; Schmitz *et al.*, 2002a; Hada *et al.*, 2003) imply that, for a certain range of parameters, the shock solutions are not static, rather reforming on the gyro scales of the incoming protons. Hybrid simulations, on the other hand, typically generate static solutions (see, e.g., Burgess *et al.*, 1989; Kucharek and Scholer, 1995; Lipatov and Zank, 1999) although

Space Science Reviews (2005) 121: 5–19
DOI: 10.1007/s11214-006-4481-x

reforming solutions are recovered for a range of values of resistivity (Quest, 1985, 1986; Hellinger *et al.*, 2002). The question then arises as to how local particle acceleration mechanisms differ between the static and time-dependent shock solutions. Here, we focus on ion acceleration in the simplest case; perpendicular supercritical shocks (see also Lee *et al.*, 2004, 2005a,b). In this paper, we first summarize the structure and dynamics of reforming shocks in an electron–proton plasma, and compare the ion energisation processes found with those known previously for steady shock solutions. We establish that the relevant spatio-temporal scales are that of the protons, and discuss scaling to astrophysical parameters. We then investigate the effect of additional pickup protons forming a shell in velocity space; and an additional thermal population of heavy ions (here, α-particles), with relevance to the heliospheric termination shock and to shocks in the solar wind and at SNR.

2. Simulation

We use a 1.5D (where scalar, and all three components of vector quantities are functions of one spatial coordinate and time) relativistic electromagnetic PIC code to simulate the structure and evolution of a supercritical, collisionless, perpendicular magnetosonic shock. Simulations of reforming shocks in quasiperpendicular and pure perpendicular geometry have been performed for example, by Scholer *et al.* (2003), who showed that the additional wavemodes supported by oblique geometry do not strongly affect the overall structure and dynamics of the reforming shock. Reforming shock solutions have also been found in higher dimensions (Lembège and Savoini, 1992). Our simulation setup for an electron–proton plasma is described in Lee *et al.* (2004), with the addition of pickup protons in Lee *et al.* (2005b); we also consider the addition of thermal α-particles, the results of which are presented for the first time here. On the particle injection boundary, the magnetic field ($B_{z,1}$) is constant and the electric field ($E_{y,1}$) is calculated self-consistently. We use the piston method to generate the shock, and shock following algorithms to obtain a sufficiently long run time, as described in Schmitz *et al.* (2002a).

To enable ion and electron time scales to be captured within the same simulation, with reasonable computational overheads we use a simulation mass ratio for ions and electrons $M_R = m_i/m_e = 20$, and ratio of electron plasma frequency to electron cyclotron frequency $\omega_{pe}/\omega_{ce} = 20$, in common with Shimada and Hoshino (2000), Schmitz *et al.* (2002a,b) and Lee *et al.* (2004). Simulations at higher mass ratios have been conducted at $M_R = 400$ (Lembège and Savoini, 2002) and at $M_R = 1{,}840$ (Scholer *et al.*, 2003); however to achieve reasonable runtimes and simulation domains, a ratio of $\omega_{pe}/\omega_{ce} = [2, \sqrt{8}]$ was used, for example, in the latter. Scholer *et al.* (2003) demonstrate that reformation is a low β process, and is not an artifact of unrealistic mass ratios, and that the differences that occur between simulations at $M_R = 20$ and $M_R = 1840$ are in the nature of the instabilities in the foot region. As we discuss later (see also Lee *et al.*, 2004, 2005a), the reflected ion dynamics are

insensitive to these instabilities. Importantly we also find the same length scales for the foot region ($\sim \lambda_{ci}$) and shock ramp ($\sim c/\omega_{pe}$) as Lembège and Savoini (2002), Scholer *et al.* (2003), thus we expect our conclusions to hold at $M_R = 1840$.

3. Shock Reformation, Thermal Proton Plasma

We begin by summarizing results for a shock in a plasma of background thermal protons and electrons only. The simulation setup is as in Lee *et al.* (2004), the shock has an Alfvénic Mach number $M_A = 10.5$, and plasma $\beta = 0.15$. The non-time-stationary nature of the reforming shock found in these simulations is shown in Figure 1, which plots $B(x, t)$. As with all figures here this is in a frame where the downstream plasma is at rest, using data collected after the shock has formed and is propagating independently of the boundary conditions. The shock can be seen to move upstream, from the right to the left over time, with the peaks in B field (the shock ramp) recurring on the time scale of the local ion cyclotron period. Over the course of each cycle the ramp forms first, then a foot region grows in front of the stationary shock ramp, whilst the shock strength is maximal. The shock structure then collapses and a new ramp (B field peak) forms $\sim 2\lambda_{ci}$ upstream, and a new cycle starts. The shock thus propagates stepwise upstream (to the left). Figures 2–4 show snapshots of the spatial distributions of the protons and

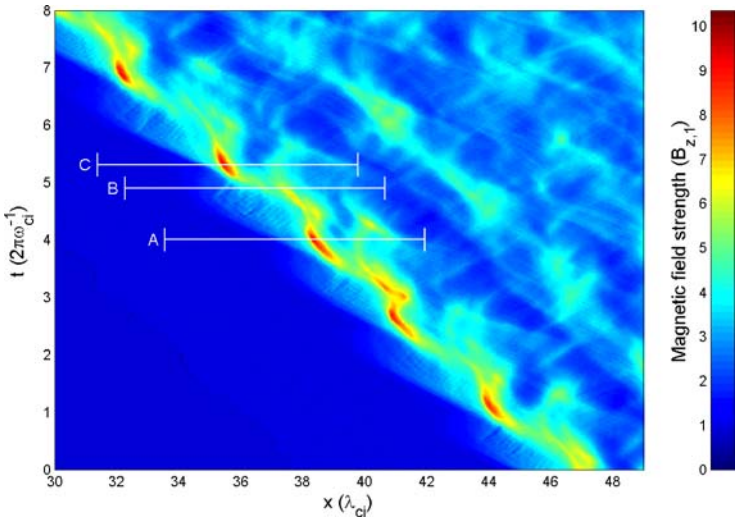

Figure 1. Evolution of perpendicular B field strength, over time (*vertical axis*, in units of upstream ion cyclotron period, $2\pi\omega_{ci}^{-1}$), and space (*horizontal axis* in units of upstream ion Larmor radii, $\lambda_{ci} = v_{inj}/\omega_{ci}$); here v_{inj} is the injection velocity, and ω_{ci} the upstream ion cyclotron frequency. The simulation snapshots in Figures 2–4 are labelled A, B and C, respectively. After Lee *et al.* (2004).

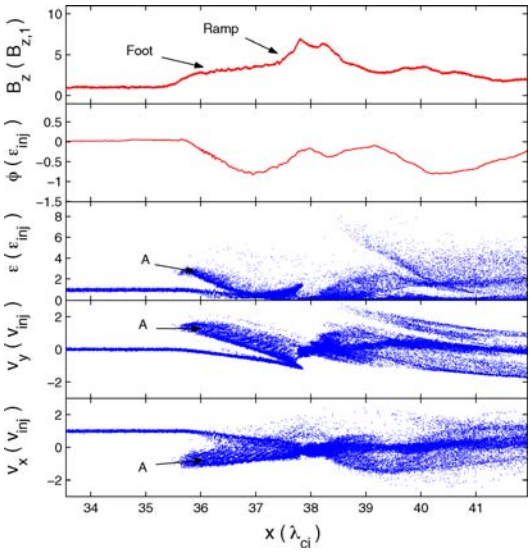

Figure 2. Cross section of the simulation in the shock region at $t = 4.0 \times 2\pi\omega_{ci}^{-1}$ (line A in Figure 1). The top panel (*Panel 1*) shows perpendicular B field, normalised to the upstream value $B_{z,1}$. *Panel 2* shows $\int E_x dx$ normalised to the ion injection energy ($\mathcal{E}_{inj}$). *Panel 3* shows the kinetic energy of the ions normalised to $\mathcal{E}_{inj}$. *Panel 4* shows the ion velocity in the y direction (perpendicular both to the shock normal and the magnetic field) normalised to injection velocity (v_{inj}). *Panel 5* shows the ion phase space (x versus v_x) with velocities normalised to v_{inj}. After Lee *et al.* (2004).

the corresponding B fields and potentials (throughout we plot B_z and minus potential, i.e. $\int E_x\, dx$ consistent with a convention used previously (Scholer *et al.*, 2003) at three different stages of the reformation cycle whose time and space co-ordinates are indicated in Figure 1 by the three white lines "A", "B" and "C". Figure 2 shows a snapshot at $t = 4 \times 2\pi\omega_{ci}^{-1}$. Ions flow in from the left hand injection boundary at v_{inj}, until they reach the shock front (currently at $38\lambda_{ci}$). At this stage of the reformation cycle the shock front is almost stationary (see Figure 1), and the ramp in the B field and potential specularly reflects a fraction of the incident ions. Consistent with a shock at rest in this frame, the ions reflect with $v_x \rightarrow -v_x$. These then move upstream into a region in front of the shock, the "foot" region (ions labelled "A"). The reflected ions form a relatively energetic population, with energies dispersed from (1–6) $\times\ \mathcal{E}_{inj}$. Figure 3 shows a later snapshot at $t = 4.9 \times 2\pi\omega_{ci}^{-1}$. The ramp region is now less well defined in the B field (see also Figure 1). In phase space, reflected protons now gyrate back towards the shock and move downstream to form the population labelled "B". By $t = 5.3 \times 2\pi\omega_{ci}^{-1}$ (Figure 4), a new ramp has formed and the reflected protons are beginning to form a new foot region as the next cycle commences. Figure 4 shows both populations of protons: those that specularly reflect to form the foot (population "A"), and those that have become energised in the foot region in the previous shock reformation cycle which now

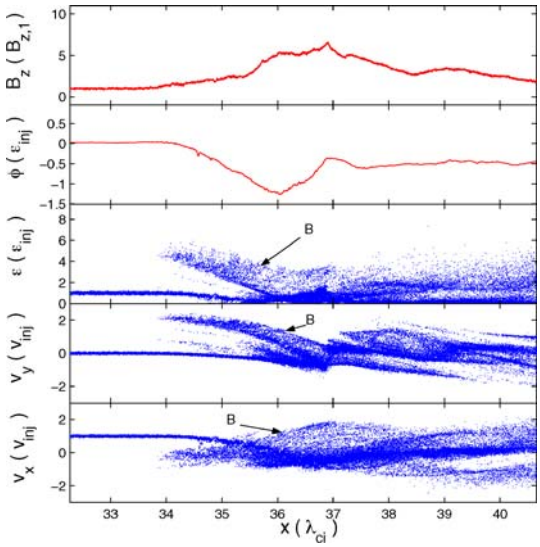

Figure 3. Cross section of the simulation in the shock region at $t = 4.9 \times 2\pi\omega_{ci}^{-1}$ (line B in Figure 1). Format as in Figure 2. After Lee *et al*. (2004).

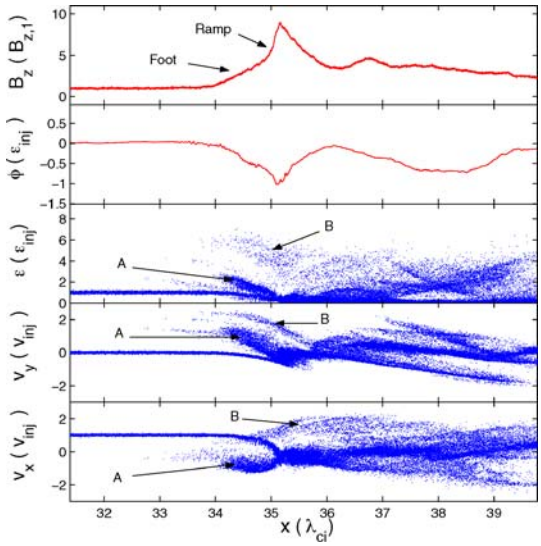

Figure 4. Cross section of the simulation in the shock region at $t = 5.3 \times 2\pi\omega_{ci}^{-1}$ (line C in Figure 1). Format as in Figure 2. After Lee *et al*. (2004).

propagate downstream (population "B"). Referring back to Figure 1, we see that a new shock has formed and is again nearly stationary in this frame.

In the reforming shock solutions, the shock then progresses in a stepwise fashion so that protons undergo specular reflection by the shock when it is temporarily at rest

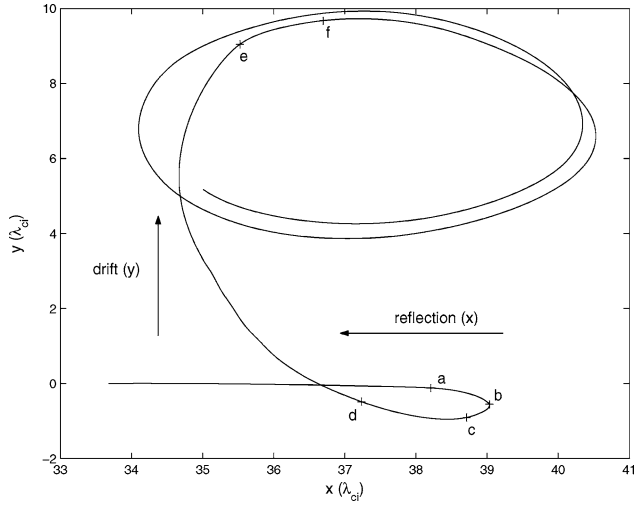

Figure 5. Position x vs. y for a high energy proton. After Lee *et al.* (2005).

in the downstream rest frame; their component of velocity normal to the shock in this frame is simply reversed. This is in contrast to the stationary shock solution in which the shock propagates steadily with constant speed v_s in the downstream rest frame (Lee *et al.*, 2004). In that frame specularly reflected ions gain approximately twice the shock speed v_s. Specularly reflected ions in the reforming shock do however gain energy in the time-dependent fields of the foot region. We now consider protons which achieve final energies downstream of $\gtrsim 6v_{\rm inj}$, close to the maximum energies reached in the above simulations. The paths of these particles have been traced though the simulation and are found to be very similar, with little dispersion in phase space as they pass through the shock (Lee *et al.*, 2004). In particular, the proton dynamics is not sensetive to structures on electron scales in the foot region (Lee *et al.*, 2005a) which have been shown to be linked to electron acceleration at shocks (Dieckmann *et al.*, 2000; Shimada and Hoshino, 2000; McClements *et al.*, 2001; Schmitz *et al.*, 2002a,b). Figure 5 shows the x–y trajectory of one of these protons, again in the downstream rest frame. The dynamics essentially comprises three stages: normal reflection from the temporarily stationary shock front into the foot region (a–c), followed by energisation during transverse drift across the shock front (d–e) and finally transmission into the downstream region (*f*), where subsequently the x component of the guiding centre velocity in the downstream rest frame is zero.

We now examine the selection mechanism for the energised protons. For a time stationary shock, Burgess *et al.* (1989) showed that protons from the extrema of the velocity space distribution upstream of the shock are preferentially reflected upstream, and so energised; whereas protons from the core of the distribution pass directly through the shock. Figure 6 shows the proton phase space (v_x and v_y vs. x)

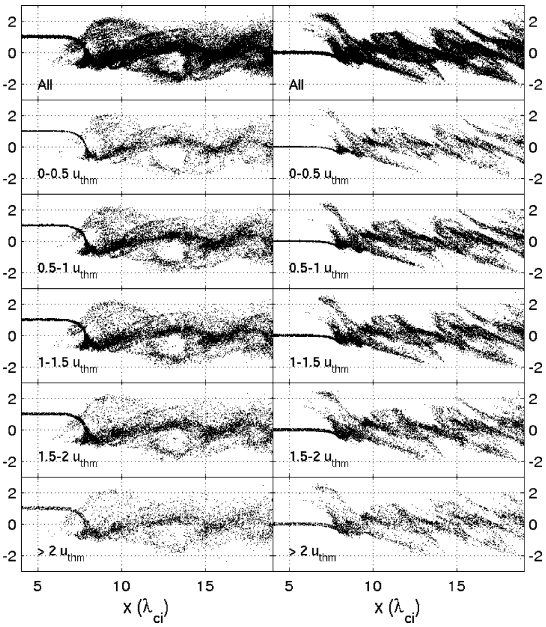

Figure 6. Phase space plots of v_x (*left*) and v_y (*right*) vs. x for particles with differing initial thermal speeds, at the instant $t = 4 \times 2\pi\omega_{\rm ci}^{-1}$. After Lee *et al*. (2005).

for groups of protons at differing initial thermal speeds, at a time when the shock ramp is maximal, and the reformation cycle has just commenced, corresponding to $t = 4 \times 2\pi\omega_{\rm ci}^{-1}$ in Figure 1 (compare with Figure 1 of Burgess *et al*., 1989). At the reforming shock a fraction of protons initially in the core of the distribution, as well as those from the tails, are now reflected back into the foot region. Whether or not a given proton is reflected depends on its normal velocity in comparison with the time-dependent shock potential. Thus, in the reforming shock the timing at which protons arrive at the shock front, as distinct from their thermal speed, determines their final location in velocity space.

These results imply that the dynamics of reflected, energised protons occur on proton Larmor scales and that details of the electron kinetics may be neglected once it is established that reforming shock solutions will occur (see Lee *et al*., 2004, 2005a, for details). Let us consider the plasma as two fluids, ions and electrons, and take the low frequency approximation: we neglect the electron inertial term and the displacement current, and assume quasi-neutrality. We also neglect the electron pressure gradient for simplicity, while anticipating that this approximation will be least reliable in the shock ramp. We obtain

$$0 \simeq \mathbf{E} + \mathbf{v}_{\rm i} \wedge \mathbf{B} + \frac{1}{\mu_0 {\rm e} n}\left[\frac{\nabla B^2}{2} - (\mathbf{B}\cdot\nabla)\mathbf{B}\right] \tag{1}$$

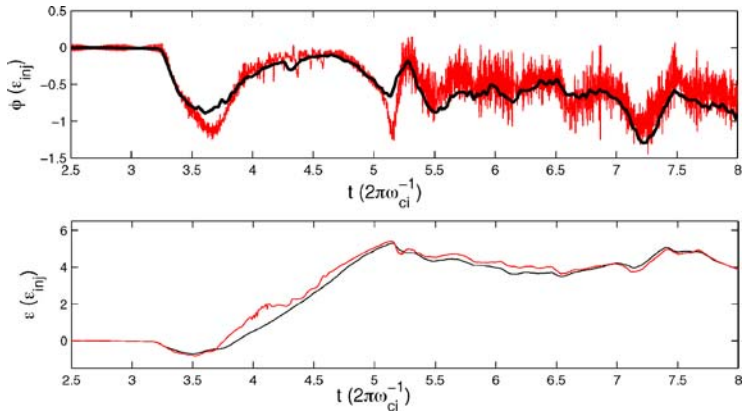

Figure 7. Lower panel: Comparison of the kinetic energy gain of the proton of Figure 5 using the PIC simulation **E** (*red*) and that on ion scales $\mathbf{E}_\mathrm{i}$ (*black*) from Equations (2). *Upper panel*: Comparison of $\int E_x\,dx$ from the PIC code (*red*), and from Equations (2) (*black*) along the trajectory. The bulk velocity $v_{\mathrm{i}x,y}$ in Equations (2) is calculated from the mean velocity of the ions within 10 grid cells $\simeq 0.02\lambda_\mathrm{ci} \simeq \lambda_\mathrm{ce}/2$ of the trajectory. After Lee *et al.* (2005a).

In the 1.5D geometry of our simulation Equation (1) simplifies since $\nabla \equiv (\partial_x, 0, 0)$ thus $(\mathbf{B}\cdot\nabla)\mathbf{B} = 0$. We also find that generally in our simulations, $v_z << v_y$, thus $(v_{\mathrm{i},y}B_z - v_{\mathrm{i},z}B_y) \simeq v_{\mathrm{i},y}B_z$. This then gives

$$E_{x,\mathrm{i}} \simeq -\frac{1}{\mathrm{en}\mu_0}\frac{\partial(B_z^2/2 + B_y^2/2)}{\partial x} - v_{\mathrm{i},y}B_z \quad \text{and} \quad E_{y,\mathrm{i}} \simeq v_{\mathrm{i},x}B_z. \tag{2}$$

Here $E_{x,\mathrm{i}}$ and $E_{y,\mathrm{i}}$ are the x, y components of the electric field in this low frequency limit. Figure 7 shows the time variation of the potential ($\int E_x\,dx$ is plotted) and the kinetic energy gain ($\int q\mathbf{E}\cdot\mathbf{v}\,dt$) of the trajectory shown in Figure 5. We apply Equations (2) to the magnetic field and particle variables from the PIC code to obtain a low frequency approximation to these which is overlaid on the values obtained directly from the PIC code. The potential from $E_{x,\mathrm{i}}$ defined in Equation (2) then essentially averages over the small-scale fluctuations of the "raw" potential from the simulation, however, the traces do not coincide where the proton interacts with the shock ramp, where ∇P_e is maximal: first during reflection at $t = 3.5-3.7\times 2\pi\omega_\mathrm{ci}^{-1}$, and subsequently during transmission to downstream at $t = 5-5.2\times 2\pi\omega_\mathrm{ci}^{-1}$. There is a close correspondence between the kinetic energy gain obtained direct from the simulation, and from the low-frequency-approximated fields, suggesting that the fine structure on electron scales does not affect the final energy gain of these protons. From Figure 7 we see that unlike the potential, the kinetic energy gain does not show a discrepancy at the shock ramp, this also suggests that the value of the potential gradient at the ramp does not contribute to the overall energy gain of these ions, provided that it is sufficient to cause reflection. This is consistent with energisation being associated with electromagnetic fields away from the ramp, the role of the

ramp potential being simply to reflect the ions. However, details of the energetics of low-energy ions that are not reflected may depend on the value of the shock ramp potential. Previous PIC simulations for a range of values of m_i/m_e (see, for example, Lembège and Savoini, 1992; Scholer *et al.*, 2003) show a variety of kinetic instabilities in the foot region, as do our results. These features occur on electron spatiotemporal scales and here we simply note that the ion dynamics will, from the above, be insensitive to these structures (see also Lee *et al.*, 2005a). The shock ramp lengthscale for these simulations at different mass ratios is similar, that is, of the order of a few c/ω_{pe} . In the remaining sections of the paper we show results from the full electromagnetic fields of the PIC simulation.

The above results imply that the characteristic time scale of shock reformation (T) and length scale of the foot region (L) are $T \simeq 1/\omega_{ci}$ and $L \simeq v_{inj}/\omega_{ci}$. After acceleration, the ions are still non-relativistic so that kinetic energy is just $\mathcal{E} = mv^2/2$. If we now consider a new set of parameters, $L \to L'$, $T \to T'$, corresponding to $m \to m'$, $B \to B'$, $v_{inj} \to v'_{inj}$, then provided that a reforming shock solution still exists for the new parameter regime it follows that $\Delta\mathcal{E}' = \Delta\mathcal{E}(m'v'^2_{inj})/(mv^2_{inj})$. Defining the injection kinetic energy as $\mathcal{E}_{inj} = mv^2_{inj}/2$ and $\mathcal{E}'_{inj} = (1/2)m'v'^2_{inj}$ this gives $\Delta\mathcal{E}'/\Delta\mathcal{E} = \mathcal{E}'_{inj}/\mathcal{E}_{inj}$. If $\Delta\mathcal{E} \sim 6\mathcal{E}_{inj}$ as found in our PIC simulations, then $\Delta\mathcal{E}' \sim 6\mathcal{E}'_{inj}$. This scaling has been confirmed by means of simulations at varying mass ratios and Mach numbers (Lee *et al.*, 2005a). For SNR, scaling the mass ratio of $M_R = m_i/m_e = 20$ to $M_R = 1{,}836$, that is, to $M_A \simeq 100$, together with a B field of $10^{-7}\,T$ and an inflow speed of $\sim 2.5 \times 10^7\,\mathrm{m\,s^{-1}}$ (Ellison *et al.*, 1999) implies that ions are injected at energies of $\sim$16 MeV by this process (Lee *et al.*, 2004).

4. Addition of Pickup Protons

The heliospheric termination shock is generated in the presence of pickup ions originating from the transheliopause interstellar medium. We have performed simulations of a perpendicular shock propagating into a collisionless plasma for conditions appropriate for the termination shock (see Lee *et al.*, 2005b, for details). The simulations are conducted as for the proton–electron plasma above, but at $M_A = 8$, an upstream solar wind thermal proton $\beta_i = 0.2$ and an electron $\beta_e = 0.5$. We include a shell distribution of 10% pickup protons, centred in velocity space on v_{inj}, with a radius $v_1 \simeq 25 \times v_{thm,SW}$, with thermal spread (Kucharek and Scholer, 1995; Zank *et al.*, 1996; Ellison *et al.*, 1999). The temporal evolution of both proton species over a single reformation cycle is shown in Figure 8. We see that the background proton dynamics proceed essentially as in the absence of the pickup protons, whereas the pickup ions form a quasi-steady extended foot region starting $\sim 6\lambda_{ci}$ upstream (see also the detailed plots of Lee *et al.*, 2005b). This can also be seen when the counts of reflected protons are compared (Lee *et al.*, 2005b).

Previous hybrid simulations provide evidence of repeated pickup proton interaction with a time-stationary shock ramp, leading to rapid ion acceleration; for

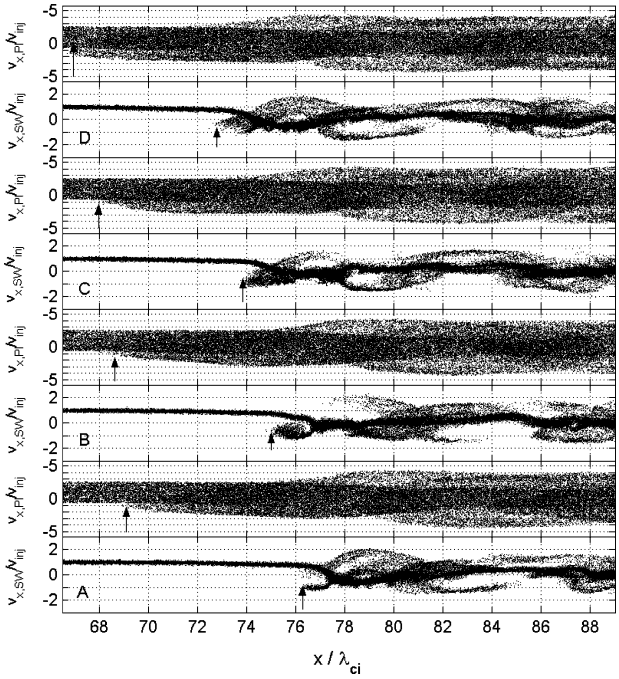

Figure 8. Phase space ($v_x/v_{\rm inj}$ vs. $x/\lambda_{\rm ci}$) for solar wind protons (*lower panel* of each pair) and pickup protons (*upper panel*) in the shock region. Four pairs of panels at equal time intervals of $0.4 \times 2\pi\omega_{\rm ci}^{-1}$ are shown starting at the lowest two panels. The maximum upstream position for the reflected ions in each species are indicated for each snapshot. After Lee *et al*. (2005b).

example, Lipatov and Zank (1999) found velocities in the y-direction of $\sim 15 v_{\rm inj}$. Figure 9 shows a series of snapshots of perpendicular velocity components through the shock region for our PIC simulations of a reforming shock (compare with Figure 2 of Lipatov and Zank, 1999). We see that in the foot region, the solar wind protons (left panels) form a reflected population which is bunched, consistent with reflection off the cyclically reforming ramp of the shock. The pickup protons (right panels) are accelerated but reach velocities $< 5 v_{\rm inj}$. This supports the conjecture (Scholer *et al*., 2003) that reforming shock solutions may be less efficient at ion acceleration processes such as shock surfing and multiple reflection. In this context, Zank *et al*. (1996) have noted that the shock ramp thickness is a critical parameter. In common with previous simulations (Shimada and Hoshino, 2000; Schmitz *et al*., 2002a) we find a shock ramp width of $\sim 2c/\omega_{\rm pe}$. However, the extension of these PIC simulations to higher dimensions, whilst retaining reforming shock solutions (Lembège and Savoini, 1992), allows wavemodes with k vectors to be oblique to the magnetic field rather than to be strictly perpendicular as in our 1.5D simulations. The occurrence of multiple reflection thus remains an open question.

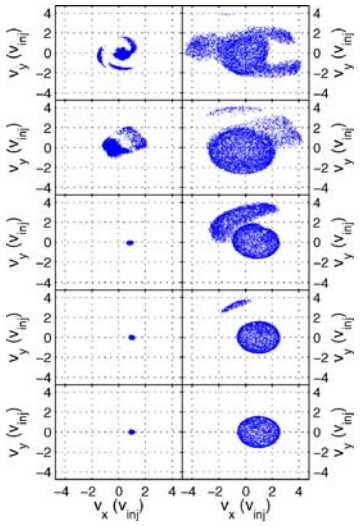

Figure 9. Results for a reforming shock: velocity distributions perpendicular to the magnetic field (v_x vs. v_y), for the solar wind protons (*left*) and pickup protons (*right*), at various positions through the simulation box. The bottom panel is $\sim 8\lambda_{ci}$ upstream of the shock front, data is then collected over $\sim\lambda_{ci}$, starting every $3\lambda_{ci}$, moving towards and through the shock.

5. Addition of Thermal α-Particles

The solar wind typically contains α-particles at 4–5% of the proton density, which can rise above 10% (Oglivie *et al.*, 1989). The plasma into which an SNR shock expands will also contain heavy ion components, especially helium, as well as protons and electrons. Observations of filaments within the Crab nebula show helium concentrations well above 50% (Henry, 1986). Here we present results of a preliminary study to investigate the effects of thermal α-particles on shock reformation. To enable comparison with previous results, these simulations are conducted using the same parameters (**B**, β, M_A, etc.) as in Section 2, but with the addition of a third ion population to represent α-particles at 4, 10 and 25% of the total ions by number density. For simplicity, in this preliminary study, α-particles have the same upstream plasma $\beta = 0.15$ as the thermal protons. Because a change in the mass density alters the Alfvén velocity, the addition of a heavy-ion component will alter the inflow velocity if the Mach number remains constant. An additional simulation has also been conducted containing 10% α-particles, but at the inflow speed used in Section 2 corresponding to $M_A = 11.4$; no significant differences with the $M_A = 10.5$ run are found. Here the ratio of α-particle to proton mass is 4, to give $m_\alpha/m_e = 80$.

Figure 10 shows the temporal evolution of the B field strength in the same format as previously for the four simulations. Panel A shows the results from the simulation detailed in Section 2 in the absence of α-particles, while Panels

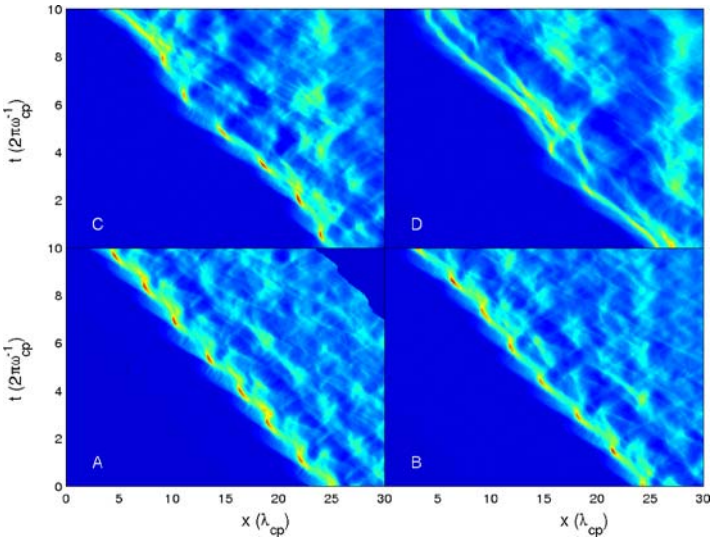

Figure 10. Evolution of perpendicular B field strength, for four simulations at various densities of α-particles, over time (*vertical axis*, in units of upstream proton cyclotron period, $2\pi\,\omega_{\rm cp}^{-1}$), and space (*horizontal axis*, normalised to $\lambda_{\rm cp} = v_{\rm inj}/\omega_{\rm cp}$). (A) A simulation in the absence of α-particles. (B) A simulation containing 4%, (C) 10% and (D) 25% α-particles. All simulations are conducted at $M_{\rm A} = 10.5$. Field strength is normalised to that upstream ($B_{z,1}$).

B, C and D show results for 4, 10 and 25% α-particles, respectively. Comparing Panels A and B of Figure 10, we see that the addition of 4% α-particles yields essentially the same shock reformation cycle. As we increase the α-particle density further, different dynamics are found, as seen in Panels C and D of Figure 10. In particular, Panel D now shows a foot-ramp structure of the shock that appears to be longer lived, so that there are intervals of time during which the shock appears to be approximately steady state, propagating more smoothly across the simulation domain. The effect on the ion energetics can be seen in the distribution functions of the ions downstream of the shock. The distribution functions shown in Figure 11 were collected over 10 upstream proton gyroperiods from a region $\sim$12–17$\lambda_{\rm cp}$ downstream of the shock front. The normalised distribution function $f(\mathcal{E})$ is shown on a semilog plot versus energies normalised to the injection energies for each species. There is some indication that as the density of α-particles increases the phase space density of high energy protons and αs also increases. These results are preliminary and in particular may be influenced by the relatively short data-collection time. We may also expect a dependence on the β of the α population. However, they suggest that the addition of heavy ions may act to introduce a longer timescale for shock reformation, thus making conditions more favourable for shock surfing and multiple reflection of the protons. Further work is needed to test this conjecture.

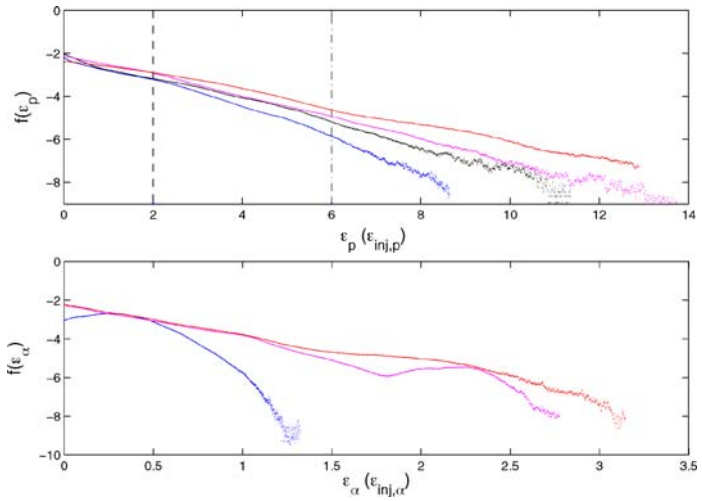

Figure 11. Energy distribution functions on a $\log_{10}$ scale for the various simulations with $M_A = 10.5$. Traces show 0% α-particles in *black*, 4% α-particles in *blue*, 10% α-particles in *magenta*, and 25% α-particles in *red*. *Upper panel*: Proton distribution functions: kinetic energy normalised to $\mathcal{E}_{\mathrm{inj},p}$. *Lower panel*: α-particle distribution functions: kinetic energy normalised to $\mathcal{E}_{\mathrm{inj},\alpha}$.

6. Conclusions

We have discussed ion acceleration in PIC simulations of a perpendicular shock, in a parameter range where the shock solutions are reforming. Our simulations self-consistently generate local ion acceleration at the shock. These ions then form an injected suprathermal population which may then be accelerated further, by other mechanisms, to cosmic ray energies. For a population of thermal background protons only, the time-dependent fields of the reforming shock are found to accelerate protons to energies up to $\sim 6\mathcal{E}_{\mathrm{inj}}$. The mechanism differs from that found in stationary shock solutions in that the accelerated protons are essentially those which first encounter the shock ramp when it is maximal. These then drift and gyrate once in the foot region, gaining energy, and are then transmitted through the shock. We have shown that the fields responsible for proton acceleration in the foot region operate on proton spatiotemporal scales and are thus able to scale our results to realistic parameters for SNR shocks. Reforming shock solutions, and the above acceleration of the thermal background protons, are found to persist in the presence of 10% pickup protons for parameters relevant to the heliospheric termination shock. The pickup protons also gain energy $\sim 20 \times \mathcal{E}_{\mathrm{inj,SW}}$, but do not appear to undergo multiple ion reflection or shock surfing, in contrast to simulations with stationary solutions. Preliminary results were also presented for simulations where thermal α-particles are added to the population of thermal background protons. Once the relative density of α-particles is increased above $\sim$10% , changes are seen in the time evolution of the shock; at $\sim$25% there are clear intervals in which

the shock dynamics become quasi-steady. These changes in the shock dynamics are accompanied by enhanced acceleration of both the proton and α-particle populations. This more realistic situation, both in the solar wind where α-particles can be present at $\sim$10%, and at SNR, where helium is observed at much higher abundances and other heavy ions are present, may be more favourable to shock acceleration.

Acknowledgements

R. E. Lee acknowledges a CASE Research Studentship from the PPARC in association with UKAEA, and a Warwick Postgraduate Research Fellowship. This work was also supported in part by the EPSRC.

References

Bell, A. R.: 1978, *MNRAS* **182**, 147–156.
Biskamp, D., and Welter, H.: 1972, *Phys. Rev. Lett.* **28**, 410–413.
Burgess, D., Wilkinson, W. P., and Schwartz, S. J.: 1989, *J. Geophys. Res.* **94**, 8783–8792.
Dieckmann, M. E., McClements, K. G., Chapman, S. C., Dendy, R. O., and Drury, L. O'C.: 2000, *Astron. Astrophys.* **356**, 377–388.
Ellison, D. C., Jones, F. C., and Baring, M. G.: 1999, *Astrophys. J.* **512**, 403–416.
Fisk, L. A., Kozlovsky, B., and Ramaty, R.: 1974, *Astrophys. J.* **190**, L35–L37.
Hada, T., Onishi, B., Lembège, B., and Savoini, P.: 2003, *J. Geophys. Res.* **108**, 1233–1244.
Hellinger, P., Trávnicek, P., and Matsumoto, H.: 2002, *Geophys. Res. Lett.* **29**, 2234–2237.
Henry, R. C. B.: 1986, *Publ. Astron. Soc. Pacific* **98**, 1044.
Kucharek, H., and Scholer, M.: 1995, *J. Geophys. Res.* **100**, 1745–1754.
Lee, R. E., Chapman, S. C., and Dendy, R. O.: 2004, *Astrophys. J.* **604**, 187–195.
Lee, R. E., Chapman, S. C., and Dendy, R. O.: 2005a, *Phys. Plasmas* **12**, 012901.
Lee, R. E., Chapman, S. C., and Dendy, R. O.: 2005b, *Ann. Geophys.* **23**, 643.
Lembège, B., and Dawson, J. M.: 1987, *Phys. Fluids* **30**, 1767–1788.
Lembège, B., and Savoini, P.: 1992, *Phys. Fluids B* **4**, 3533–3548.
Lembège, B., and Savoini, P.: 2002, *J. Geophys. Res.* **107**, 1037–1055.
Leroy, M. M., Winske, D., Goodrich, C., Wu, C. S., and Papadopoulos, K.: 1982, *J. Geophys. Res.* **87**, 5081.
Lever, E. L., Quest, K. B., and Shapiro, V. D.: 2001, *Geophys. Res. Lett.* **28**, 1367–1370.
Lipatov, A. S., and Zank, G. P.: 1999, *Phys. Rev. Lett.* **82**, 3609–3612.
McClements, K. G., Dieckmann, M. E., Ynnerman, A., Chapman, S. C., and Dendy, R. O.: 2001, *Phys. Rev. Lett.* **87**, 25.
Oglivie, K. W., Coplan, M. A., Bochsler, P., and Geiss, J.: 1989, *Solar Phys.* **124**, 167.
Pesses, M. E., Jokipii, J. R., and Eichler, D.: 1981, *Astrophys. J.* **246**, L85–L88.
Quest, K. B.: 1985, *Phys. Rev. Lett.* **54**, 1872–1874.
Quest, K. B.: 1986, *J. Geophys. Res.* **91**, 8805.
Rice, W. K. M., Zank, G. P., Richardson, J. D., and Decker, R. B.: 2000, *Geophys. Res. Lett.* **27**, 509–512.
Schmitz, H., Chapman, S. C., and Dendy, R. O.: 2002a, *Astrophys. J.* **570**, 637–646.
Schmitz, H., Chapman, S. C., and Dendy, R. O.: 2002b, *Astrophys. J.* **579**, 327–336.

Scholer, M., Shinohara, I., and Matsukiyo, S.: 2003, *J. Geophys. Res.* **108**, 1014–1024.
Shimada, N., and Hoshino, M.: 2000, *Astrophys. J.* **543**, L67–L71.
Zank, G. P., Pauls, H. L., Cairns, I. H., and Webb, G. M.: 1996, *J. Geophys. Res.* **101**, 457–477.
Zank, G. P., Rice, W. K. M., Le Roux, J. A., and Matthaeus, W. H.: 2001, *Astrophys. J.* **556**, 494–500.